Dalton Transactions

PAPER

Cite this: *Dalton Trans.*, 2015, **44**, 18527

Synthesis and crystal structure of a new hexagonal perovskite 7H-$Ba_7Li_{1.75}Mn_{3.5}O_{15.75}$ with Mn^{4+}/Mn^{5+} charge distribution†

N. V. Tarakina,*[a,b] A. P. Tyutyunnik,[c] G. V. Bazuev,[c] A. D. Vasilev,[d] C. Gould,[b] I. V. Nikolaenko[c] and I. F. Berger[c]

Received 22nd April 2015,
Accepted 28th September 2015

DOI: 10.1039/c5dt01528f

www.rsc.org/dalton

$Ba_7Li_{1.75}Mn_{3.5}O_{15.75}$ is a new hexagonal perovskite whose crystal structure has elements typical for the layered hexagonal perovskites and quasi-one-dimensional oxides, hence representing a new polytype. It has been synthesized *via* a solid-state microwave route. The crystal structure was solved using a combination of X-ray and neutron diffraction data, which show that $Ba_7Li_{1.75}Mn_{3.5}O_{15.75}$ crystallizes in a hexagonal unit cell with parameters a = 5.66274(2) Å and c = 16.7467(1) Å (V = 465.063(4) Å^3), with one formula unit, and can be described as columns of face-shared octahedra occupied by Mn^{4+} and Li^+ cations and vacancies along the c axis separated in the ab plane by barium atoms. Every sixth layer, the coordination of Mn^{5+} and Li^+ changes to tetrahedral. Additional local ordering of manganese and lithium atoms among cationic sites leading to the formation of a rhombohedral supercell has been observed by scanning transmission electron microscopy.

Introduction

In the last two decades, manganese perovskite-like compounds have been intensively researched because of their unique electronic and magnetic properties. Among others the alkaline-earth manganites $AMnO_3$ (A = Ca, Sr, Ba) are particularly interesting as multiferroic materials. In this context, it is worth mentioning the prediction of a ferroelectric ground state in the cubic perovskites $AMnO_3$ (A = Ca, Ba),[1] the discovery of spontaneous electric polarization and magnetic ordering in the solid solution $Sr_{1-x}Ba_xMnO_3$ at $x \geq 0.45$,[2] strong magnetoelectric effects near room temperature in single-crystal $BaMnO_{2.99}$ and its derivatives $BaMn_{0.97}M_{0.03}O_3$ (M = Li, K)[3] and the discovery of collinear-magnetism-driven ferroelectricity in the Ising chains of Ca_3CoMnO_6.[4,5] This broad variety of properties stems not only from different chemical compositions but also from the various crystal structures in which manganites crystallize. Understanding the crystal structures of existing compounds and designing compounds with new structural types are main objectives of present-day research on manganites.

From a structural point of view, binary oxides of alkaline-earth elements and manganese with the composition $AMnO_3$ (A = Ca, Sr, Ba) belong to different perovskite-structure types.[6,7] The ideal perovskite ABO_3 has a cubic unit cell (sp. gr. $Pm\bar{3}m$, Z = 1) and can be described as the A cation occupying the 12-fold coordination site between corner-sharing BO_6 octahedra. However, the ideal cubic form rarely occurs. For example, the structure of $SrMnO_3$ has different modifications and the one closest to that of an ideal perovskite forms either at very high temperatures with subsequent oxidation at 350 °C in air[8] or as the result of high-pressure/high-temperature treatment.[9] $CaMnO_3$ produced by replacement of the Sr^{2+} cations by the smaller Ca^{2+} cations has a rhombic distorted-perovskite structure with sp. gr. *Pnma*, featuring corner-shared MnO_6 octahedra.[6]

If some of the "cubic" layers in a perovskite are shifted over (1/3, 2/3, 0) from their positions, "hexagonal" layers form resulting in a so-called hexagonal perovskite structure. The structure of a hexagonal perovskite ABO_3 is more easily described as a superposition (along the c axis) of close-packed AO_3 layers in the octahedral voids of which (formed by oxygen anions) B element atoms are located.[6,10] Depending on factors like cation sizes, temperature, pressure, oxygen stoichiometry and substitution of B cations by other elements, the sequence

[a]*The NanoVision Centre, School of Engineering and Materials Science, Queen Mary University of London, Mile End, London E1 4NS, UK. E-mail: n.tarakina@qmul.ac.uk*
[b]*Experimentelle Physik III, Physikalisches Institut and Wilhelm Conrad Röntgen – Research Centre for Complex Material Systems, Universität Würzburg, Am Hubland, D-97074 Würzburg, Germany*
[c]*Institute of Solid State Chemistry, Ural Branch of the Russian Academy of Sciences, 91 Pervomayskaya, 620990 Ekaterinburg, Russia*
[d]*L.V. Kirensky Institute of Physics, Siberian Branch of the Russian Academy of Sciences, 50 Akademgorodok, 660036 Krasnoyarsk, Russia*
†Electronic supplementary information (ESI) available. See DOI: 10.1039/c5dt01528f

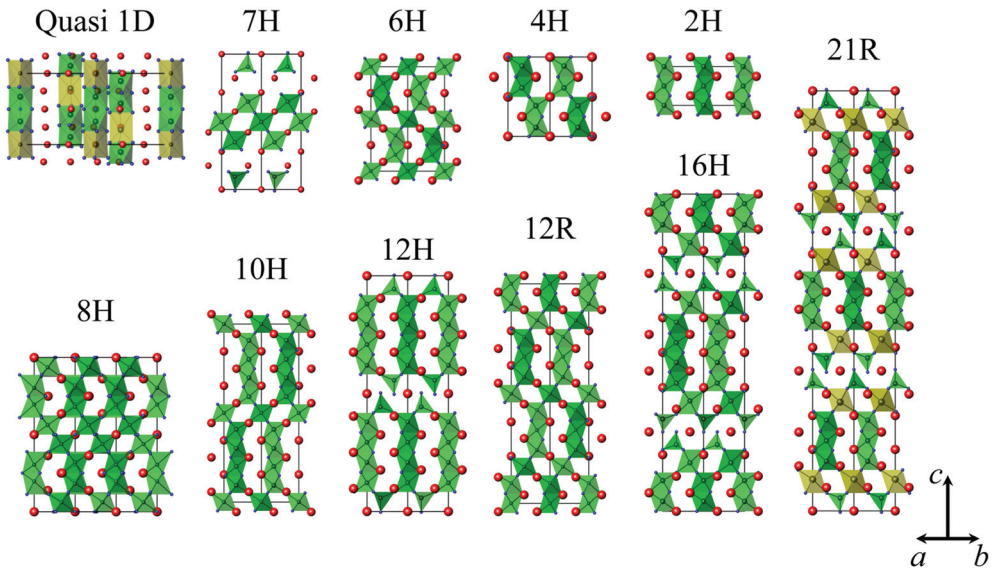

Fig. 1 Crystal structures of $BaMnO_3$: different polytypes and quasi-one-dimensional (quasi-1D) compounds $A_4A'Mn_2O_9$. Red and blue spheres indicate A cation and oxygen sites, respectively. Positions indicated by green and yellow polyhedra are preferably occupied by manganese and A′ atoms, respectively.

of alternation of cation layers can change; as a result, polytypes characterized by various ratios of hexagonal (usually denoted as h) and cubic layers (c) are formed. For example, at moderate temperatures $SrMnO_3$ crystallizes in a 4H structure (sp. gr. $P6_3/mmc$, $Z = 4$) at ambient pressure and a 6H hexagonal structure (sp.gr. $P6_3/mmc$, $Z = 6$) at 6 GPa.[8,11,12]

Another example is $BaMnO_3$: in stoichiometric form it has a hexagonal 2H structure (sp. gr. $P6_3/mmc$, $Z = 2$, Fig. 1) containing only face-shared octahedra along the c axis.[13] Oxygen-deficient $BaMnO_{3-\delta}$ forms hexagonal/rhombohedral polytypes with different ratios of cubic corner-shared and hexagonal face-shared layers.[14] With the use of the high-pressure/high-temperature synthesis method and by replacing manganese by other elements the size and valence of which are different from those of manganese, it is possible to obtain 4H-$BaMnO_{3-x}$ ($0 \le x \le 0.35$),[15] 6H-$Ba_{0.7}Sr_{0.3}Ru_{1-x}Mn_xO_3$ ($0.2 \le x \le 0.4$),[16] 7H-$Ba_7Nb_4MoO_{20}$,[17] 8H-$Ba_8Ta_6NiO_{24}$,[18] 10H-$Ba_5Sn_{1.1}Mn_{3.9}O_{15}$,[19] 12H-$(BaSr)_{0.5}Mn_4Cr_2O_{17}$,[20] 9R-$BaRu_{1-x}Mn_xO_3$ ($0 \le x \le 0.90$),[21] 12R-$Ba_3NdMn_2O_9$,[22] 16R-$Ba_4Ca_{1-x}Mn_{1+x}O_{12-\delta}$,[23] 21L-$Ba_7Ca_2Mn_5O_{20}$ [24] and other structural types. The crystal structures of some hexagonal/rhombohedral polytypes are shown in Fig. 1.

Interestingly, substitution of the Mn^{4+} cations in $BaMnO_3$ by cations of elements with smaller valence gives rise to hexagonal perovskites with mixed or enhanced average degree of oxidation of manganese. So, the complex oxide $Ba_4Ca_{1-x}Mn_{3+x}O_{12-y}$ has a rare 16-layer or closely related structure with ordered oxygen vacancies and tetrahedral layers.[23] The octahedral and tetrahedral positions are occupied by manganese cations in different oxidation states. This oxide and the 21-layer manganite $Ba_7Ca_2Mn_5O_{20}$ obtained recently[24] can be described as members of a new family of layered structures of the general formula $Ba_{5+n}Ca_2Mn_{3+n}O_{3n+14}$. Structural analysis and magnetic measurements suggests that the octahedra in $Ba_7Ca_2Mn_5O_{20}$ are occupied by Mn^{4+} cations and the tetrahedra by Mn^{5+} cations. It is worth to mention that the mixed valence state Mn^{4+}/Mn^{5+} was also described in the hexagonal 6-layer perovskite $Ba_3ErMn_2O_9$,[25] as well as in the quasi-one-dimensional compounds $Ba_4NaMn_2O_9$,[26] and $Sr_4LiMn_2O_9$,[27] (Fig. 1, quasi-1D). However, no evidence for the existence of individual atomic positions of the manganese cations Mn^{4+} and Mn^{5+} in the structure of these compounds have been found. The structure of $Ba_3ErMn_2O_9$ consists of dimers of face-shared octahedra and corner-shared octahedra. The structure of the quasi-one-dimensional compounds $Ba_4NaMn_2O_9$ and $Sr_4LiMn_2O_9$ belongs to the family of 2H perovskites, which are characterized by 1D columns of face-shared MnO_6 octahedra and $Na(Li)O_6$ prisms arranged in the (oct–oct–prism) sequence and isolated through $Ba^{2+}(Sr^{2+})$ cations.

In this work we aimed to synthesise a new quasi-one-dimensional complex oxide with the "$Ba_4LiMn_2O_9$" composition. In fact, our detailed structural study showed that the aimed overall composition "$Ba_4LiMn_2O_9$" corresponds to the chemical formula $Ba_7Li_{1.75}Mn_{3.5}O_{15.75}$ (*i.e.* by multiplying the overall composition "$Ba_4LiMn_2O_9$" by a factor of 7/4). Below we report the synthesis, detailed structural investigations and measurements of magnetic properties of this new complex cation-deficient perovskite, $Ba_7Li_{1.75}Mn_{3.5}O_{15.75}$.

Experimental

In this work we used a microwave muffle furnace with a nominal generator power of 700 W and a frequency of

2450 MHz. The furnace is equipped with heating rods, which heat up to the required temperature by absorbing electromagnetic energy. A chromel-alumel thermocouple located in the space between the rods was used for temperature control. The thermocouple has a cover made of non-corrosive steel, which protects against the electromagnetic field.

A mixture of the initial reagents $BaCO_3$ (99.9%), Li_2CO_3 (99.99%) and MnO_2 (99.9%) with ratio equal to the stoichiometry of $Ba_4LiMn_2O_9$ was prepared. It was preliminarily calcined at 950 °C for 1 hour in the microwave furnace. Then the product was ground, pressed with pressure 3000 kg cm^{-2} into a pellet, and annealed at 1030 °C for 2 hours with intermediate grinding after 1 hour of annealing.

X-ray powder diffraction (XRD) patterns were collected at the "X-ray structure analysis" centre for collective use at the Institute of Solid State Chemistry, Ural Branch of the Russian Academy of Sciences (Ekaterinburg, Russia) at room temperature on a STADI-P (STOE) diffractometer in transmission geometry with a linear mini-PSD detector using CuKα_1 radiation in the 2θ range from 2 to 120° with a step of 0.02°. Polycrystalline silicon (a = 5.43075(5) Å) was used as an external standard. Neutron diffraction data were collected at room temperature in the 2θ range 5–120° with a step of 0.05° and neutron wavelength λ = 1.5265 Å using the D2A setup of the reactor IVV 2M (Zarechny, Russia). Possible impurity phases were checked by comparing XRD patterns with those in the PDF2 database (ICDD, USA, Release 2009).

The crystal structure of the obtained compound was refined with simultaneous use of X-ray and neutron powder diffraction data using the GSAS software.[28,29] The peak profiles were fitted with a pseudo-Voigt function $I(2\theta) = x\mathrm{L}(2\theta) + (1 - x)\mathrm{G}(2\theta)$ (where L and G are the Lorentzian and Gaussian parts, respectively). The angular dependence of the peak width was described by the relation $(\mathrm{FWHM})^2 = U_{tg^2}\theta + V_{tg}\theta + W$, where FWHM is the full line width at half maximum. The background level was described by a combination of thirty-sixth-order Chebyshev polynomials. The absorption correction function for a flat-plate sample in transmission geometry was applied.[28,29]

The scanning electron-microscopic images and the energy-dispersion X-ray microanalysis (EDX) spectra were obtained with a Gemini Zeiss scanning electron microscope equipped with an X-max 50 mm^2 SDD energy-dispersion X-ray detector. The scanning transmission electron microscopy study was performed using a FEI (S)TEM Titan 80-300 microscope, operated at 300 kV. For the (S)TEM study an ethanol suspension of the sample was prepared and kept in an ultrasonic bath for 5 minutes; then a drop of this suspension was put onto a holey carbon film supported on a Cu grid.

The magnetic measurements were carried out on an MPMS-5-XL SQUID magnetometer produced by QUANTUM DESIGN. A 0.2 g sintered sample was placed into a gelatin capsule. The temperature was varied from 3 to 300 K. The applied magnetic field was 0.3 kOe.

Density measurements were carried out on the AccuPyc II 1340 Gas Displacement Pycnometry System (Micromeritics, USA) with sample chamber volume 0.1 cm^3. About 30–50% of the chamber volume was filled by the powder sample, 15 measurements were done.

Results and discussion

Crystal structure

The sample obtained as the result of microwave treatment of a mixture with overall composition "$Ba_4LiMn_2O_9$" is a deep-green crystalline powder. In this respect it should be noted that $Sr_4LiMn_2O_9$ is deep-brown[27] and $Ba_3Mn_2O_8$ is green.[30] The size of the crystals is typical of the powder produced by solid-phase synthesis (1 μm or larger). According to the EDX data, the Ba/Mn ratio was found to be 2.12, *i.e.* close to 2. The small deviation from the perfect Ba/Mn ratio can be explained by the presence of about 2% of $BaCO_3$ in the obtained powder as calculated during full-profile fitting of XRD and NPD data.

The XRD pattern of the obtained compound was indexed in hexagonal symmetry with unit cell parameters a = 5.66274(2) Å and c = 16.7467(1) Å (V = 465.063(4) Å^3). Since no systematic absences have been observed, all primitive trigonal space groups can be chosen. As a first step, based on the similarity of the overall composition "$Ba_4LiMn_2O_9$" to $Sr_4LiMn_2O_9$, an attempt to adopt a quasi-1D model of the crystal structure[27] was tried, where columns of face-sharing octahedra and trigonal prisms occupied by manganese and lithium atoms and oriented along the c axis are separated by barium (strontium) atoms. But it failed, giving very bad correspondence to the XRD data.

Significant improvement of the fitting was achieved when one barium atom was moved to the origin, cutting the columns in short strings of five octahedra. At the same time, one manganese atom was moved from the column into the vacated space, obtaining a tetrahedral oxygen coordination. For the resulting model the $P\bar{3}m1$ (164) space group was chosen. To get more accurate positions of lithium and oxygen atoms, the neutron data were refined simultaneously with the XRD data. Weak reflections of $BaCO_3$ were fitted as a second phase during the refinement, and its fraction was calculated to be 2 mass%.

Since the number of barium atoms in the unit cell was found to be 7, the structural formula has to be written as $Ba_7Li_{1.75}Mn_{3.5}O_{15.75}$, *i.e.* by multiplying the overall composition "$Ba_4LiMn_2O_9$" by a factor of 7/4. The measured density, 5.0760(65) g cm^{-3}, lies within two standard deviations from 5.062 g cm^{-3} calculated for this composition with one formula unit in the unit cell. Fig. 2 shows experimental, theoretical, and difference X-ray and neutron powder diffraction patterns for a $Ba_7Li_{1.75}Mn_{3.5}O_{15.75}$ sample. The results of crystal structure refinement, selected interatomic distances and angles for $Ba_7Li_{1.75}Mn_{3.5}O_{15.75}$ are listed in Tables 1, 2 and 3, respectively. The almost perfect fit of the XRD data indicates correct positions of the barium atoms, whose X-ray scattering power is significantly higher than that of manganese, oxygen and lithium. However, the small imperfections in the fit of the neutron data implied some problems with the model. Introducing mutual

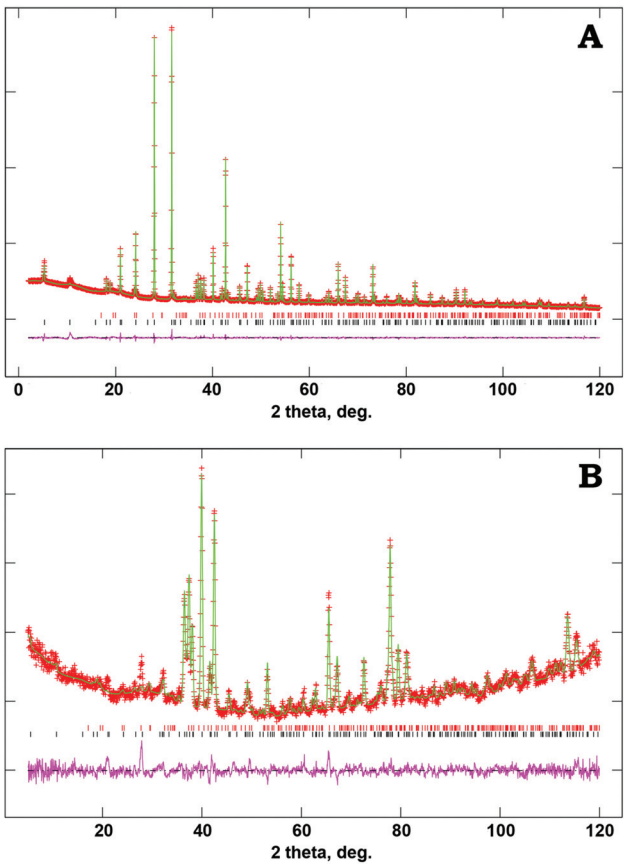

Fig. 2 Observed (crosses), calculated (solid line) and difference (bottom line) X-ray (a) and neutron (b) powder diffraction patterns of $Ba_7Li_{1.75}Mn_{3.5}O_{15.75}$ with $BaCO_3$ as the impurity phase. Red and black lines show the positions of the peaks of $Ba_7Li_{1.75}Mn_{3.5}O_{15.75}$ and $BaCO_3$, respectively.

occupation of octahedral and tetrahedral sites by manganese and lithium gave a slight reduction in *R*-factors. An additional improvement of the fit was achieved by refining the occupations of oxygen sites. One has to note that, according to the

Table 1 Crystallographic data for $Ba_7Li_{1.75}Mn_{3.5}O_{15.75}$

Structural formula	$Ba_7Li_{1.75}Mn_{3.5}O_{15.75}$
Formula unit	1
Space group	$P\bar{3}m1$ (164)
$a = b$, Å	5.66274(2)
c, Å	16.7467(1) Å
α, β, γ, °	90, 90, 120
V, Å^3	465.063(4)
Calculated density, g cm^{-3}	5.062
Measured density, g cm^{-3}	5.0760(65)
Radiation	X-ray, λ = 1.54056 Å
	Neutrons, λ = 1.5265 Å
T, K	298
R-Factors (X-ray)	wR_p = 2.17%, R_p = 1.56%, $R(F^2)$ = 5.52%
R-Factors (neutrons)	wR_p = 2.76%, R_p = 2.11%, $R(F^2)$ = 15.08%

structural formula $Ba_7Li_{1.75}Mn_{3.5}O_{15.75}$ instead of the ideal $Ba_7(Li,Mn)_7O_{20}$, there should be some vacancies in the structure, since only 5.25 atoms occupy 7 sites available for manganese and lithium, and 15.75 oxygen atoms occupy 20 available sites. The formula calculated based on the full-profile structure refinement is $Ba_7Li_{3.14(9)}Mn_{3.86(9)}O_{16.8(2)}$. The number of lithium atoms clearly exceeds the expected value 1.75. Since the scattering power of lithium and vacancies are nearly equal for X-ray radiation, and close for neutron radiation, the distribution of vacancies is expected to follow the distribution of lithium atoms. In the following discussion, a mixture of lithium atoms and vacancies will be implied where it says lithium atoms.

The remaining discrepancy, a manifestation of the average nature of the model shown in Fig. 3(a–d), has been clarified by electron microscopy studies.

Only the positions of the main reflections in the selected area electron diffraction (SAED) patterns can be indexed within the model proposed from the XRD and neutron data (Fig. 4, red indices). Supercell spots with weak lines of diffuse scattering present in the pattern taken along $[1\bar{1}0]_{P\bar{3}m1}$ clearly indicate an increase in the *a* parameter of the primitive unit cell and a rotation of the hexagonal axes by 30°. New reflection conditions (*hkl*: $-h + k + l = 3n$; *h* − *hl*: $h + l = 3n$; *hhl*: $l = 3n$;

Table 2 Atomic coordinates and isotropic thermal parameters (U_{iso} × 100, Å^2) for $Ba_7Li_{1.75}Mn_{3.5}O_{15.75}$

Atom		*x*/*a*	*y*/*b*	*z*/*c*	Fraction	U_{iso} × 100
Ba(1)	1a	0.0	0.0	0.0	1.0	3.6(1)
Ba(2)	2d	1/3	2/3	0.5724(2)	1.0	2.63(9)
Ba(3)	2d	2/3	1/3	0.6964(2)	1.0	2.3(1)
Ba(4)	2d	1/3	2/3	0.8263(1)	1.0	1.9(1)
Mn/Li(1)	2c	0.0	0.0	0.3509(4)	0.79/0.21(1)	3.9(2)[a]
Mn/Li(2)	1b	0.0	0.0	1/2	0.67/0.33(1)	3.9(2)[a]
Mn/Li(3)	2d	2/3	1/3	0.9085(6)	0.80/0.20(1)	3.9(2)[a]
Mn/Li(4)	2c	0.0	0.0	0.194(2)	0.005/0.995(8)	3.9(2)[a]
O(1)	6i	0.1785(8)	0.8215(8)	0.1307(4)	0.88(1)	1.73(8)[a]
O(2)	6i	0.8443(8)	0.689(2)	0.5677(5)	0.718(8)	1.73(8)[a]
O(3)	6i	0.1511(7)	0.302(1)	0.7083(4)	1.0	1.73(8)[a]
O(4)	2d	2/3	1/3	0.004(1)	0.59(2)	1.73(8)[a]

[a] Thermal parameters of manganese/lithium and oxygen atoms were constrained as single variables, respectively.

Table 3 Selected interatomic distances d (Å) and angles (°) for $Ba_7Li_{1.75}Mn_{3.5}O_{15.75}$

Interatomic distances			Interatomic distances		
Ba(1)–O(1)	6×	2.803(6)	Ba(3)–O(1)	3×	3.270(6)
Ba(1)–O(4)	6×	3.2702(4)	Ba(3)–O(2)	3×	2.772(9)
Average		3.037	Ba(3)–O(3)	6×	2.8425(6)
Expected[a]		2.97	Average		2.932
			Expected[a]		2.97
Ba(2)–O(2)	6×	2.8345(4)	Ba(4)–O(1)	6×	2.924(2)
Ba(2)–O(2)	3×	2.922(10)	Ba(4)–O(3)	3×	2.665(7)
Ba(2)–O(3)	3×	2.895(7)	Ba(4)–O(3)	1×	2.835(19)
Average		2.872	Average		2.837
Expected[a]		2.97	Expected[a]		2.88
Mn/Li(1)–O(2)	3×	2.048(10)	Mn/Li(3)–O(1)	3×	1.665(8)
Mn/Li(1)–O(3)	3×	1.782(8)	Mn/Li(3)–O(4)	1×	1.606(19)
Mn/Li(2)–O(2)	6×	1.902(8)	Mn/Li(4)–O(1)	3×	2.042(21)
			Mn/Li(4)–O(3)	3×	2.213(29)
O(1)–Mn/Li(3)–O(1)	3×	105.3(4)	O(1)–Mn/Li(3)–O(4)	3×	113.4(4)

[a] The sum of the crystal radii according to ref. 31: Ba^{+2}(X) – 1.66 Å, Ba^{+2}(XII) – 1.75 Å, O^{-2}(III) – 1.22 Å.

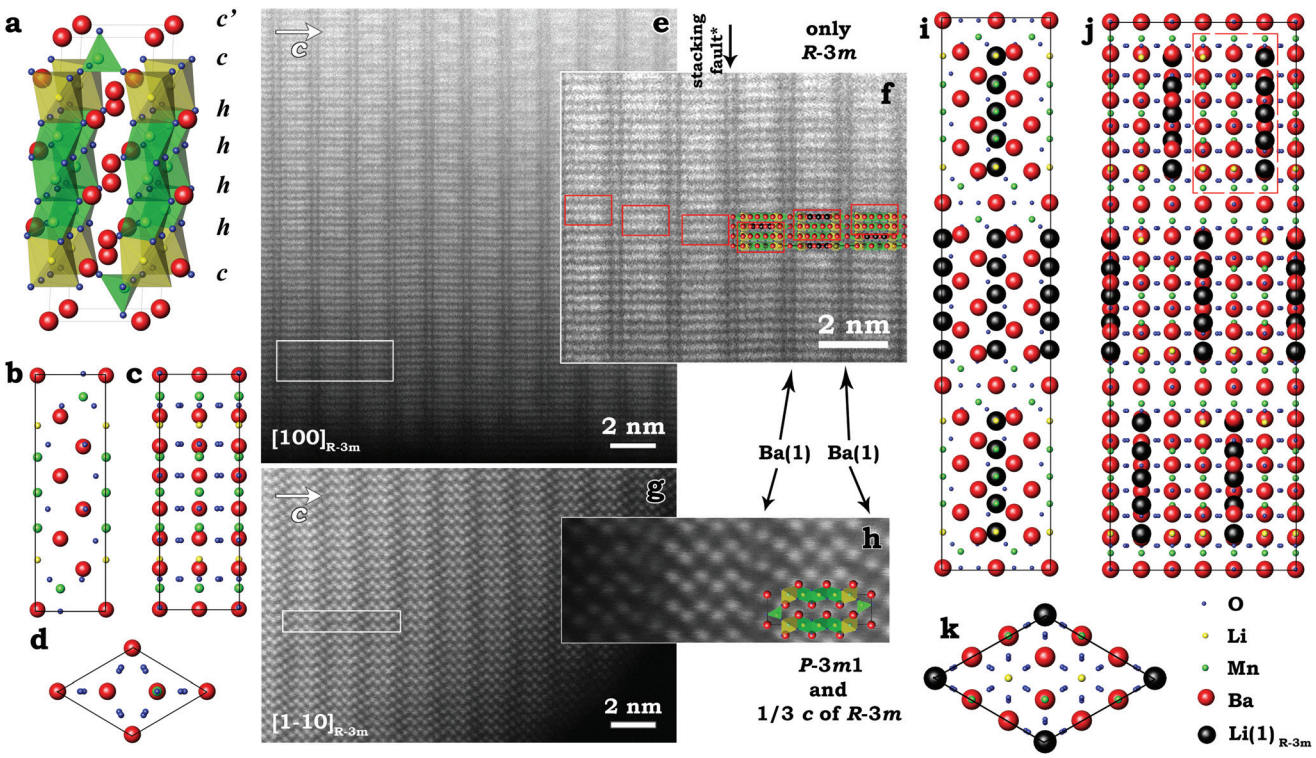

Fig. 3 (a) Schematic drawing of the average structure of $Ba_7Li_{1.75}Mn_{3.5}O_{15.75}$ obtained from powder diffraction data. Letters c, h denote [BaO_3] and c' denotes [BaO_2]. Projection of (a) on $(110)_{P\bar{3}m1}$ (b), on $(100)_{P\bar{3}m1}$ (c), on $(001)_{P\bar{3}m1}$ (d). HAADF-STEM images taken along $[100]_{R\bar{3}m}$ (e) and $[1\text{–}10]_{R\bar{3}m}$ (g) directions in the crystal. Enlargements from (e) with the rhombohedral superstructure cell superimposed to indicate atomic positions and red rectangles showing the positions of the blocks of layers (Ba/Li + Ba/Mn + Ba/Mn) with different intensity (f). Enlargements from (g) with the $P\bar{3}m1$ unit cell placed to indicate atomic positions. Schematic drawing of the rhombohedral superstructure of $Ba_7Li_{1.75}Mn_{3.5}O_{15.75}$ in projections on $(110)_{R\bar{3}m}$ (i), $(1\text{–}10)_{R\bar{3}m}$ (j) and $(001)_{R\bar{3}m}$ (k). Red and blue spheres indicate barium and oxygen sites, respectively. Positions indicated by green and yellow spheres are preferably occupied by manganese and lithium atoms, respectively. Black spheres indicate lithium/manganese sites mainly occupied by lithium. The contrast enhancement in (g) from bottom to top is due to the continuous increase of crystal thickness.

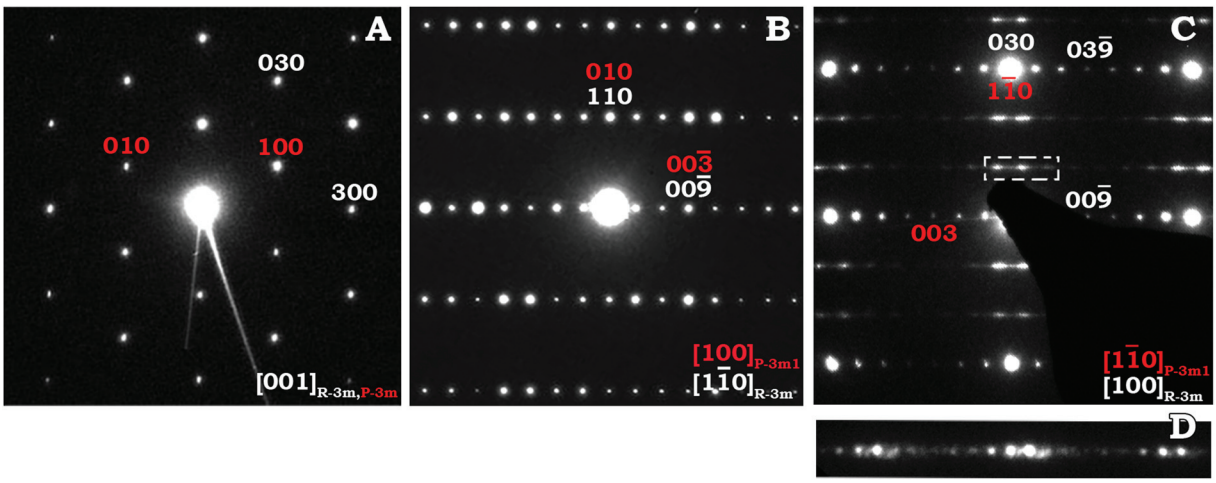

Fig. 4 (a–c) Selected area electron diffraction patterns taken along the main zone axis in the crystal. (d) Enlargement from the dashed area in (c). Red and white indices correspond to primitive and rhombohedral centred lattices, respectively.

00l: $l = 3n$) indicate the formation of a rhombohedrally centered lattice (five possible space groups: $R3$ (146), $R\bar{3}$ (148), $R32$ (155), $R3m$ (160), $R\bar{3}m$ (166)) with unit cell parameters a = 10 Å, c = 51.3 Å. Weak lines of diffuse scattering going through supercell reflections along the c^* direction indicate the presence of stacking disorder in the structure. In order to clarify the origins of ordering within the *ab* plane in the crystal and diffuse scattering present in the SAED patterns, HRSTEM experiments were performed. In Fig. 3(e–h), HAADF-STEM images taken along the $[100]_{R\bar{3}m}$ and $[1{-}10]_{R\bar{3}m}$ directions in the crystal are shown. Layers occupied by Ba(1) atoms are marked with black arrows, the positions of these atoms are in perfect agreement with the model proposed from powder diffraction data. In between, 6 layers occupied by Ba, Mn and Li are present, forming columns along the c direction. The contrast on the HAADF-STEM images is dependent only on the atomic number of the elements in the crystal ($\sim Z^2$) and its thickness. White dots arranged in a zigzag manner in Fig. 3(g and h) correspond to Ba(2), Ba(3) and Ba(4) positions; in between these zigzag columns, Mn and Li atoms are placed as shown in Fig. 3(i). A rotation over 30 degrees around the c axis leads to an overlapping of barium, manganese and lithium columns, Fig. 3(g and j). According to the structural model obtained from XRD all atomic columns along the $[1{-}10]_{P\bar{3}m1}$ ($[100]_{R\bar{3}m}$ direction) should give equal contrast on the HAADF-STEM images. Instead, two columns of higher intensity alternate with one column of lower intensity. The observed difference in contrast suggests ordering of metal atoms within the *ab* plane. We believe that the two columns of dots with high intensity result from the overlapping of scattering signals from Mn and Ba atoms, while one column of dots with lower intensity is the sum of Ba and Li signals. However, additional annular bright-field imaging or atomic-column resolved Li-K edge spectrum imaging experiments are required to obtain a full description of the supercell. Here and in the following we will refer to such a set of three columns as one block (marked with dashed lines in Fig. 3(f and j)). The described cation ordering explains the increase of the a parameter of the unit cell by $\sqrt{3}$ and a rotation of the crystal axes by 30° with respect to the primitive trigonal lattice, Fig. 3(j and k).

A periodic stacking of blocks along the c direction with shifts equal to 2/3 of the width of the block would result in a perfect rhombohedral supercell, Fig. 3(e, f, i–k, stacking fault). However, in addition to shifts over 2/3, occasional shifts over 1/3 (= −2/3) have been observed, destroying the perfect rhombohedral symmetry of the crystal and causing the presence of diffuse streaks in the SAED patterns along the $[100]_{R\bar{3}m}$ direction as well as problems with refining X-ray and neutron powder data using the supercell model. The structure can be described either through the formation of twin planes perpendicular to the c direction or through stacking faults along the c direction. A description through the formation of twin planes partly helps to understand the intensity distributions and periodicity with which supercell reflections appear on the SAED patterns (Fig. 4(d)). One should note that such local ordering could not be accounted for in the full-profile fitting of XRD and neutron data using the big rhombohedra supercell, since diffraction reflections corresponding to a smaller averaged subcell are only observed there.

To place $Ba_7Li_{1.75}Mn_{3.5}O_{15.75}$ within the large family of hexagonal perovskites one can calculate the ratio between the parameter c (16.74667 Å) and the average thickness of the BaO_3 layer (2.4 Å).[24] If we consider the c value obtained from X-ray and neutron structure refinement then it is equal to 6.975; therefore the structure of this oxide can be related to that of the hexagonal perovskite 7H polytype. Among 7H perovskites, one compound of the composition $Ba_7Nb_4MoO_{20}$ is also known to crystallize in the $P\bar{3}m1$ space group with lattice parameters a = 5.8644(2) Å and c = 16.5272(4) Å.[17] The existence of two empty cationic positions (Fig. 5) is probably the reason for the formation of this unusual polytype.

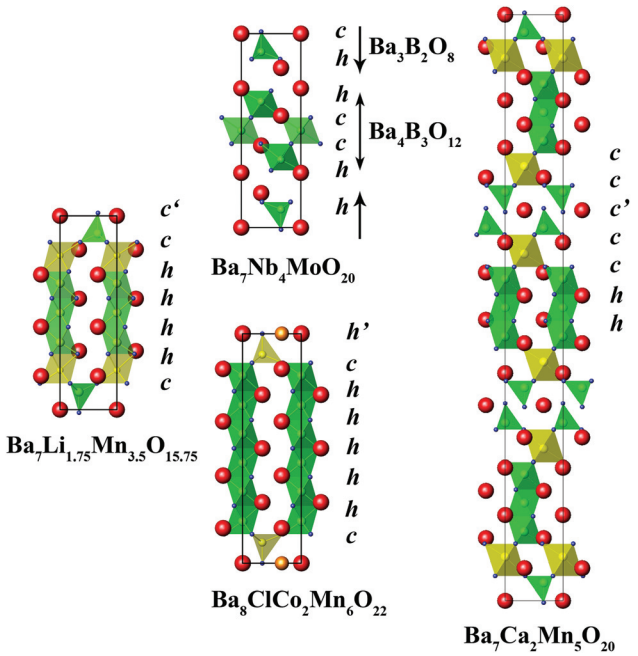

Fig. 5 Schematic drawing of the average structure of: $Ba_7Li_{1.75}Mn_{3.5}O_{15.75}$ obtained from powder diffraction data, $Ba_7Nb_4MoO_{20}$,[17] $Ba_8ClCo_2Mn_6O_{22}$ [32] and $Ba_7Ca_2Mn_5O_{20}$.[24] Positions indicated by green spheres are preferably occupied by Mn, Mn/Li or Nb/Mo atoms. Positions indicated by yellow spheres are occupied by Li, Co or Ca. Red spheres indicate barium atoms, blue spheres indicate oxygen atoms. Letters *c*, *h* denote [BaO_3], and *c*′ and *h*′ denote [BaO_2] and [$BaOCl_{1-x}$], respectively.

The structure of $Ba_7Nb_4MoO_{20}$ can be described as comprising of a [111] perovskite block of corner-shared octahedra with composition $Ba_4B_3O_{12}$ and a block of composition $Ba_3B_2O_8$, where Nb^{5+}/Mo^{6+} cations are distributed in quasi-regular tetrahedral polyhedra (Fig. 5). Nominally, $Ba_7Li_{1.75}Mn_{3.5}O_{15.75}$ can also be described as a 7-layer hexagonal perovskite as shown above. The face-shared octahedra alternate with manganese and lithium cations forming columns along the *c* axis separated by barium atoms. This structure resembles the quasi-one-dimensional oxides, in which octahedra and trigonal prisms alternate along the *c* axis (Fig. 1). But in $Ba_7Li_{1.75}Mn_{3.5}O_{15.75}$, the lithium-manganese octahedron in each seventh layer is replaced by a barium polyhedron with 6 oxygen atoms at a distance of 2.77 Å and with 6 more oxygen atoms at a distance of 3.27 Å. In turn, the position of the barium polyhedron in the space between the columns is occupied by a lithium-manganese tetrahedron. As a result, the unit cell of hexagonal $Ba_7Li_{1.75}Mn_{3.5}O_{15.75}$ contains 7 oxygen layers.

Recently Iorgulescu *et al.*[32] reported the formation of a new 8H-$Ba_8Co_2Mn_6ClO_{22}$ quasi-1D hexagonal perovskite, which consists of 6 face-sharing octahedral layers and 2 tetrahedral layers (Fig. 5). Interestingly, the stabilisation of this compound was shown to be likely due to Mn/Co ordering in the octahedral and tetrahedral sites, respectively (disorder in Mn/Co results in the well-known 5H[33] and 12H[34] polytypes), Fig. 1. We believe that in the case of $Ba_7Li_{1.75}Mn_{3.5}O_{15.75}$, ordering of Li and Mn^{4+}/Mn^{5+} cations can be one of the main factors, which allowed to stabilise the new hexagonal 7H polytype. Another reasons for the formation of this polytype are likely to be the small size of the Li^+ cations (compared to Na^+ in $Ba_4NaMn_2O_9$, Fig. 1, quasi-1D), the large size of the Ba^{2+} cations (compared to Sr^{2+} in $Sr_4LiMn_2O_9$) and the high oxidation state of half of the manganese cations (5+). In the structure of $Ba_7Li_{1.75}Mn_{3.5}O_{15.75}$, Mn^{4+} and Li^+ cations are located in the octahedra forming 5 layers along the *c* axis of the unit cell. Considering that the average oxidation state of manganese is +4.5, it is probable that Mn^{5+} cations occupy mainly the tetrahedral positions with one Mn–O distance of 1.606(19) Å and the other three distances being 1.665(8) Å. The average Mn–O distance (1.65 Å) in the tetrahedra is somewhat smaller than the bond length in $Sr_4LiMn_2O_9$ (1.68 Å).[27] The interatomic distances in the octahedra constituting the layers with predominant manganese content (1.902(8) Å) are within the typical values for Mn^{4+} in the octahedral oxide positions.[35,36] The average interatomic distances in the octahedra with a large content of lithium (2.13 Å) are close to the typical bond lengths (2.035–2.152 Å) for the octahedral position of Ln_2LiIrO_6 perovskites (Ln = La, Pr, Nd, Sm, Eu).[37]

If we consider the *c* value obtained from electron microscopy studies then the ratio between the parameter *c* and the average thickness of the BaO_3 layer (2.4 Å) is equal to 21.37 and therefore we can also compare the structure of $Ba_7Li_{1.75}Mn_{3.5}O_{15.75}$ with that of the 21L hexagonal polytype (in particular $Ba_7Ca_2Mn_5O_{20}$). In $Ba_7Ca_2Mn_5O_{20}$, instead of having four layers of corner-sharing MnO_6 octahedra (specific for ideal 21L hexagonal perovskites), a block of two layers of CaO_6 octahedra and two layers of MnO_4 tetrahedra exists (Fig. 5). Similarly, in $Ba_7Li_{1.75}Mn_{3.5}O_{15.75}$, there are two layers of mixed Li/Mn octahedra preferably occupied by Li and two layers of Mn/Li tetrahedra preferably occupied by Mn. In addition, ordering of Mn and Li atoms in *ab* planes doubles the *a* parameter of $Ba_7Li_{1.75}Mn_{3.5}O_{15.75}$ compared to that of $Ba_7Ca_2Mn_5O_{20}$. The separation of Mn^{4+} and Mn^{5+} cations in the atomic position in the structure suggest carrying out a magnetic study.

Magnetic measurements

The results of static magnetic susceptibility measurements at H = 0.3 kOe for $Ba_7Li_{1.75}Mn_{3.5}O_{15.75}$ at 3–300 K are shown in Fig. 6. As follows from the inset in Fig. 6, in the temperature range 100–220 K the magnetic susceptibility χ obeys the Curie–Weiss law $\chi = C/(T - \theta)$, where χ is the magnetic susceptibility, C is the Curie constant (4.20 cm^3 K mol^{-1}), and θ is the Weiss temperature ($\theta = -55$ K). Deviations of the dependence of $1/\chi = f(T)$ from a straight line are observed above 220 K and below 100 K. The experimental value of the effective magnetic moment (μ_{eff}) for $Ba_7Li_{1.75}Mn_{3.5}O_{15.75}$ (5.80μ_B) is close to the theoretical moment (6.34μ_B) calculated in the assumption that all manganese is present as $Mn^{4+}(S = 3/2)/Mn^{5+}(S = 1)$ cations at ratio 1 : 1. The Weiss temperature θ has a negative value,

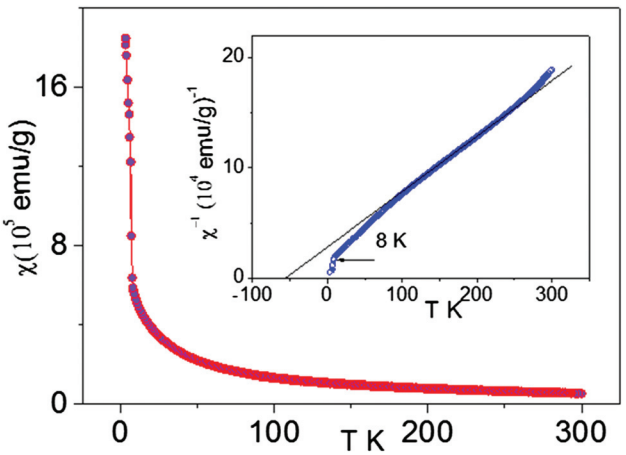

Fig. 6 Temperature dependence of the magnetic susceptibility χ for $Ba_7Li_{1.75}Mn_{3.5}O_{15.75}$ (H = 0.3 kOe). The inset shows the $\chi^{-1} = f(T)$ dependence.

which is indicative of prevailing antiferromagnetic exchange between magnetic moments.

The deviation of the $\chi = f(T)$ dependence for quasi-one-dimensional oxides $A_4A'Mn_2O_9$ from the Curie–Weiss law is due to structural features of the compounds, in particular, to the presence of exchange-bound dimers from magnetic cations Mn^{4+}, which occupy face-shared octahedrons. This is attested by a broad maximum at 40–150 K that was observed in the $\chi = f(T)$ dependence for the series $Sr_4AMn_2O_9$ (A = Li, Zn, Ni, Cu).[27,38–40]

Their magnetic properties were discussed in the framework of a model of isotropic antiferromagnetic ordering between exchange-bound dimers from Mn^{4+} cations against a background weak inter-chain interaction. It is probable that the deviation of the dependence $1/\chi = f(T)$ from the Curie–Weiss law at high and low temperatures points to the similar mechanism of antiferromagnetic exchange interaction between the manganese paramagnetic ions in $Ba_7Li_{1.75}Mn_{3.5}O_{15.75}$ (Fig. 6). The low level of manganese and lithium structural ordering in octahedra and the presence of high-valence paramagnetic Mn^{5+} cations in tetrahedral positions are the reasons for the observed differences. For the determination of the reason of the sharp χ increase below 8 K, additional investigations are necessary.

Conclusions

A new complex cation-deficient perovskite, $Ba_7Li_{1.75}Mn_{3.5}O_{15.75}$, with mixed manganese valence Mn^{4+}/Mn^{5+} and distinct distribution of these ions in the structural positions has been synthesized. Its crystal structure contains features typical for the layered hexagonal perovskites and quasi-one-dimensional oxides and represents a new polytype. The face-shared octahedra occupied by Mn^{4+} and Li^+ cations and vacancies form columns along the *c* axis separated by barium atoms. Moreover, the unit cell of $Ba_7Li_{1.75}Mn_{3.5}O_{15.75}$ includes tetrahedral layers occupied by Mn^{5+} and Li^+ cations. A local ordering of manganese and lithium atoms among cationic sites leading to a rhombohedral supercell formation has been detected.

Acknowledgements

N.V.T. acknowledges funding by the Bavarian Ministry of Sciences, Research and the Arts. X-ray powder diffraction studies were carried out at the Center for collective use "X-ray structure analysis" at the Institute of Solid State Chemistry, Ural Branch of RAS (Ekaterinburg, Russia).

References

1 S. Bhattacharjee, E. Bousquet and P. Ghosez, *Phys. Rev. Lett.*, 2009, **102**, 117602.
2 H. Sakai, J. Fujioka, T. Fukuda, D. Okuyama, D. Hashizume, F. Kagawa, H. Nakao, Y. Murakami, T. Arima, A. Q. R. Baron, Y. Taguchi and Y. Tokura, *Phys. Rev. Lett.*, 2011, **107**, 137601.
3 O. Korneta, T. F. Qi, M. Ge, M. S. Parkin, L. E. De Long, P. Schlottmann and G. Cao, *J. Phys.: Condens. Matter*, 2011, **23**, 435901.
4 V. G. Zubkov, G. V. Bazuev, A. P. Tyutyunnik and I. F. Berger, *J. Solid State Chem.*, 2001, **160**, 293.
5 Y. J. Choi, H. T. Yi, S. Lee, Q. Huang, V. Kiryukhin and S.-W. Cheong, *Phys. Rev. Lett.*, 2008, **100**, 047601.
6 A. F. Wells, *Structural Inorganic Chemistry*, 5th edn, Clarendon Press, Oxford, 2012.
7 F. S. Galasso, *Structure and Properties of Inorganic Solids*, Pergamon Press, Oxford, 1970, p. 176.
8 A. A. Belik, Y. Matsushita, Y. Katsuya, M. Tanaka, T. Kolodiazhnyi, M. Isobe and E. Takayama-Muromachi, *Phys. Rev. B: Condens. Matter*, 2011, **84**, 094438.
9 Y. Syono, S. Akimoto and K. J. Kohn, *Phys. Soc. Jpn.*, 1969, **26**, 993.
10 J. Darriet and M. A. Subramanian, *J. Mater. Chem.*, 1995, **5**, 543.
11 P. D. Battle, T. C. Gibb and C. W. Jones, *J. Solid State Chem.*, 1988, **74**, 60.
12 B. L. Chamberland, A. W. Sleight and J. F. Weiher, *J. Solid State Chem.*, 1970, **1**, 506.
13 E. J. Cussen and P. D. Battle, *J. Solid State Chem.*, 2000, **12**, 831.
14 J. J. Adkin and M. A. Hayward, *Chem. Mater.*, 2007, **19**, 755.
15 J. J. Adkin and M. A. Hayward, *J. Solid State Chem.*, 2006, **179**, 70.
16 C. Yin, G. Li, J. Lin and J. P. Attfield, *Chem. – Asian J.*, 2009, **4**, 969.
17 E. Garcia-Gonzalez, M. Parras and J. M. Gonzalez-Calbet, *Chem. Mater.*, 1999, **11**, 433.

18 R. V. Shpanchenko, L. Nistor, G. Van Tendeloo, J. Van Landuyt, S. Amelinckx, A. M. Abakumov, E. V. Antipov and L. M. Kovba, *J. Solid State Chem.*, 1995, **114**, 560.
19 C. Yin, G. Li, T. Jin, J. Tao, J. Richardson, C.-K. Loong, F. Liao and J. Lin, *J. Alloys Compd.*, 2010, **489**, 152.
20 J. H. Clark and M. A. Hayward, *Chem. Mater.*, 2008, **20**, 4612.
21 C. Yin, G. Li, W. A. Kockelmann, J. Lin and J. P. Attfield, *Phys. Rev. B: Condens. Matter*, 2009, **80**, 094420.
22 H. Yang, Y. K. Tang, L. D. Yao, Z. Zhang, Q. A. Li, F. Y. Lia, C. Q. Jin and R. C. Yu, *J. Alloys Compd.*, 2007, **432**, 283.
23 N. Floros, C. Michel, M. Hervieu and B. Raveau, *Chem. Mater.*, 2000, **12**, 3197.
24 N. Floros, C. Michel, M. Hervieu and B. Raveau, *J. Solid State Chem.*, 2002, **168**, 11.
25 C. Rabbow and H. Müller-Buschbaum, *Z. Naturforsch.*, 1994, **498**, 1277.
26 E. Quarez, P. Roussel, O. Pérez, H. Leligny, A. Bendraoua and O. Mentré, *Solid State Sci.*, 2004, **6**, 631.
27 G. V. Bazuev, A. P. Tyutyunnik, I. F. Berger, I. V. Nikolaenko and B. G. Golovkin, *J. Alloys Compd.*, 2011, **509**, 6158.
28 B. H. Toby, *J. Appl. Crystallogr.*, 2001, **34**, 210.
29 A. C. Larson and R. B. Von Dreele, General Structure Analysis System (GSAS), Los Alamos National Laboratory Report LAUR, 2004, 86–748.
30 S. Manna, S. Majumder and S. K. De, *J. Phys.: Condens. Matter*, 2009, **21**, 236005.
31 R. D. Shannon, *Acta Crystallogr., Sect. A: Fundam. Crystallogr.*, 1976, **32**, 751.
32 M. Iorgulescu, H. Kabbour, N. Tancret, O. Mentré and P. Roussel, *ChemComm*, 2010, **46**, 5271.
33 L. Miranda, J. Ramírez-Castellanos, A. Varela, J. González-Calbet, M. Parras, M. Hernando, M. T. Fernández-Díaz and M. García Hernández, *Chem. Mater.*, 2007, **19**, 1503.
34 L. Miranda, A. Feteira, D. C. Sinclair, M. García Hernández, K. Boulahya, M. Hernando, A. Varela, J. M. González-Calbet and M. Parras, *Chem. Mater.*, 2008, **20**, 2818.
35 C. A. Moore and P. D. Battle, *J. Solid State Chem.*, 2003, **176**, 88.
36 V. G. Zubkov, A. P. Tyutyunnik, I. F. Berger, V. I. Voronin, G. V. Bazuev, C. A. Moore and P. D. Battle, *J. Solid State Chem.*, 2002, **167**, 453.
37 M. J. Davis, M. D. Smith, K. E. Stitzer and H.-C. zur Loye, *J. Alloys Compd.*, 2003, **351**, 95.
38 G. V. Bazuev, V. N. Krasilnikov and D. G. Kellerman, *J. Alloys Compd.*, 2003, **352**, 190.
39 A. El Abed, E. Gaudin, J. Darriet and M.-H. Whangbo, *J. Solid State Chem.*, 2002, **163**, 513.
40 G. V. Bazuev, N. A. Zaitseva, V. N. Krasilnikov and D. G. Kellerman, *Russ. J. Inorg. Chem.*, 2003, **48**, 219.